Supporting Information

A monolithic Co-$FeCo_8S_8$ electrode for stable anion exchange membrane water electrolyzer driven by fluctuating power supply

Jahangir Khan[#], Heming Liu[#], Tianhao Zhang, Xin Kang, Zhiyuan Zhang, Yuxiao Dong, Shanlin Li, Jiarong Liu, Qiangmin Yu[*], and Bilu Liu

Shenzhen Geim Graphene Center, Shenzhen Key Laboratory of Advanced Layered Materials for Value-added Applications, Institute of Materials Research, Tsinghua Shenzhen International Graduate School, Tsinghua University, Shenzhen 518055, PR China

[#]These authors contributed equally: Jahangir Khan, and Heming Liu

Corresponding author

[*]E-mail: yu.qiangmin@sz.tsinghua.edu.cn (QM)

Experimental section

Material preparations

For the synthesis of the Co-$FeCo_8S_8$ electrode, all chemicals were utilized without further purification. Co foam samples were cut into 1×1.5 cm^2 (pore size of 0.1-0.2 mm, thickness of 1 mm, Kunshan Jiayisheng Electronics Co., Ltd., China) and subjected to a cleaning process. First, the Co foam underwent sonication in a 1 M HCl aqueous solution for 30 minutes followed by washing with deionized water. Secondly, FeS_2 powder was put into a mortar grinder (Retsch RM 200, Germany) to get a fine powder. Then the obtained powder was dispersed into ethanol and kept under sonication for 30 minutes to make a well-dispersed solution. After this, the dispersion with a mass loading of 5 mg FeS_2 was dropped on Co foam. The sample was subsequently placed in a glass tube with a vacuum of 10^{-3} Pa. Finally, the vacuum-sealed glass tube was subjected to annealing in a furnace at 750 °C for 4 hours. Under high-temperature vacuum annealing, FeS_2 precursor and Co foam chemically reacted with each other to form a new phase of Co-$FeCo_8S_8$. After that, the chronopotentiometry (CP) test at 500 mA cm^{-2} was applied in 1M KOH electrolyte to totally activate the Co-$FeCo_8S_8$ electrode for 2 hours, thus achieving the Co-FeCoOOH electrode. For the synthesis of Co-IrO_2 electrode, commercial IrO_2 with a mass loading of 4 mg cm^{-2} was drop-casted on a Co foam for electrochemical tests, and on a Co foil for micro-scratch tests. The IrO_2 ink consisted of 50 mg IrO_2 powder (Sinero Tech. Co., China, 10g), 8 mL isopropanol, 1.5 mL deionize d water and 0.5 mL Nafion binder (Dupont Co., 5 wt%).

Materials characterizations.

The crystalline structure analysis was performed using X-ray diffraction (XRD, Rigaku, SmartLab 9KW, Japan). To explore the surface morphology and determine the elemental composition, scanning electron microscopy (SEM, ZEISS Sigma300, USA) was employed. Atomic structures were characterized by spherical aberration corrected transmission electron microscopy (TEM, Thermo Scientific Spectra 300, USA) with an accelerating voltage of 300 kV. Raman spectra were collected using a 532 nm laser excitation (Horiba LabRAM HR Evolution, Japan). Chemical analysis was performed by

high resolution X-ray photoelectron spectroscopy (XPS, PHI5000VersaProbeII, Japan). The X-ray absorption spectroscopy (XAS) spectra were collected at the BL11B beamline situated within the Shanghai Synchrotron Radiation Facility. The mechanical property of the electrodes was characterized by micro scratch tester (Anton Paar, UNHT, Austria). The contact angle was tested by contact angle meter (KRUSS DSA30, Germany).

Electrochemical measurements.

All electrochemical measurements were executed using an electrochemical workstation (Zahner Zennium Pro, Germany). Throughout the tests, a 1.0 M KOH electrolyte solution was employed. For the experimental setup, a standard three-electrode cell configuration was adopted, utilizing the Hg/HgO electrode as the reference electrode and the Pt foil as the counter electrode. To minimize solution resistance, the working and reference electrodes were positioned nearby, ensuring it remained below 0.3 Ω. To ensure a fair and consistent comparison across samples, the wetted area of all tested electrodes was uniformly tailored to 1 cm^2. The applied potential was transformed using the following equation:

$$E_{vs\ RHE} = E_{vs\ Hg/HgO} + 0.059 * pH + 0.098$$

LSV was executed utilizing a scan rate of 1 mV s^{-1}, coupled with an 85% iR correction. CV experiments were conducted at a scan rate of 50 mV s^{-1}. For CP test, current densities of 2,000, 1,000, and 500 mA cm^{-2} were employed during the stability assessments. EIS was carried out at a potential corresponding to a current density of 10 mA cm^{-2}, encompassing frequencies ranging from 1 MHz to 0.1 Hz. The ECSA was determined by evaluating the electrochemical double-layer capacitances (C_{dl}) of the catalysts. The calculation of ECSA was performed using the subsequent formula.

$$ECSA = C_{dl}/C_s$$

The electrochemical double-layer capacitance of the working electrodes denoted as C_{dl}, and the specific capacitance of the electrode materials (C_s) was adopted as 0.04 mF cm^{-2} in 1M KOH. In light of the potential reconstruction of catalysts, the measurement of electrochemical double-layer capacitance was conducted after the OER process.

Device fabrication & test

The activated Co-FeCoOOH electrode was used as an anode and the FeMoNi catalyst was used as a cathode to construct the anion exchange membrane water electrolyzer (AEMWE). The FeMoNi catalyst was prepared according to the previously reported method[1]. The mass loading of both anode and cathode was 5 mg cm^{-2}. Sustanion X37-50 Grade RT membrane was adopted as AEM in our protocol. There were no extra steps needed for the AEMWE assembly, such as heating and pressing. Using a potentiostat (Zahner XC, Germany), we investigated the AEMWE performance in 1.0 M KOH at 20 °C and 6.0 M KOH at 80 °C. The polarization curve was obtained by LSV protocol with a scan rate of 10 mV s^{-1}. The durability test was conducted by CP at a current density of 500 mA cm^{-2} for more than 400 hours in 1.0 M KOH at 20 °C. The temperature was regulated using an electrolyte heater. The degradation of potential (D_v) during stability test was calculated by subtracting final potential from initial potential and divided by the total time of stability. The AST protocol includes high current density operation, loading cycling and OCV states, which is beneficial for understanding the degradation mechanisms of different materials and components used in AEMWE. In detail, the protocol includes cyclic CP with a period of 500-100-20-0-20-100-500 mA cm^{-2}, each cycle running for 6 minutes. The electrolyte was collected each hour during AST and constant CP for quantitatively analyzing the dissolution content of Fe and Co element using ICP-OES. The actual dissolved amount was obtained by subtracting the electrolyte impurity content from the test results. The higher dissolution content of Fe and Co in the first 6 hours is due to electrode activation.

Micro-scratch mechanical test

The micro-scratch test is to apply a normal force on the surface of the material to produce a scratch and measure the mechanical properties of the material. A diamond tip was applied to the surface of the material with an initial load of 0.01 N, and then the load was gradually increased until the end load of 1N. In this process, the tip would progressively scratch a certain distance on the surface of the material. The scratch length is 3 mm and the sliding rate is 6 mm min^{-1}. Acoustic emission technology with acquisition rate of 30 Hz was

applied to monitor crack propagation. For sample preparation, almost identical coating thickness should be ensured and recommended to be below 5 μm. The thickness of Co-FeCoOOH and Co-IrO_2 were 1.15±0.04 and 1.01±0.03 μm, respectively, as shown in Fig. S4

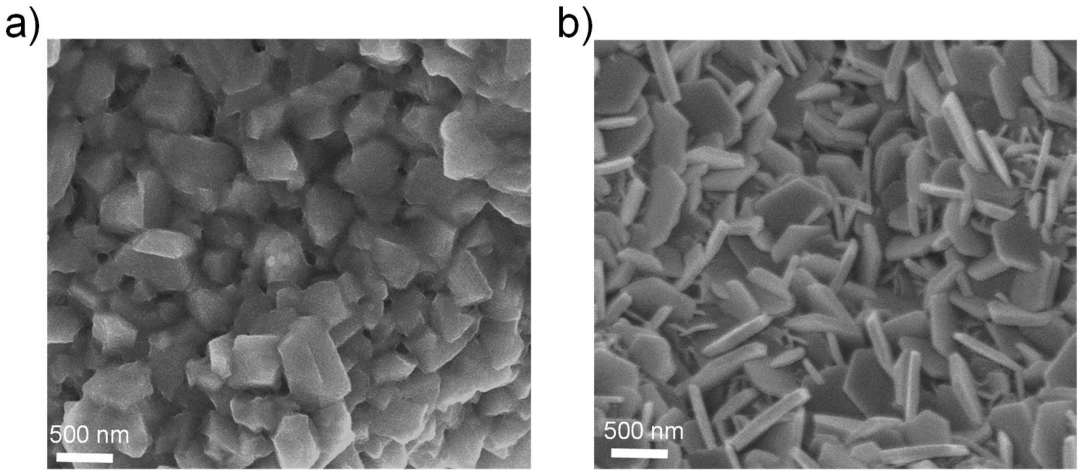

Figure S1. The SEM images of (a) Co-$FeCo_8S_8$ and (b) Co-FeCoOOH.

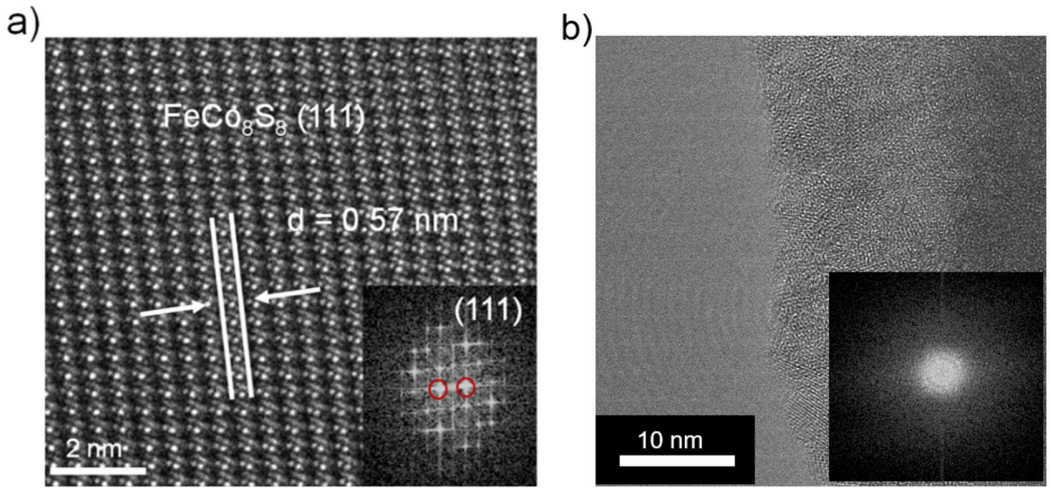

Figure S2. HRTEM images of Co-$FeCo_8S_8$ (a) and Co-FeCoOOH (b) on the surface. The inset images are the corresponding FFT patterns.

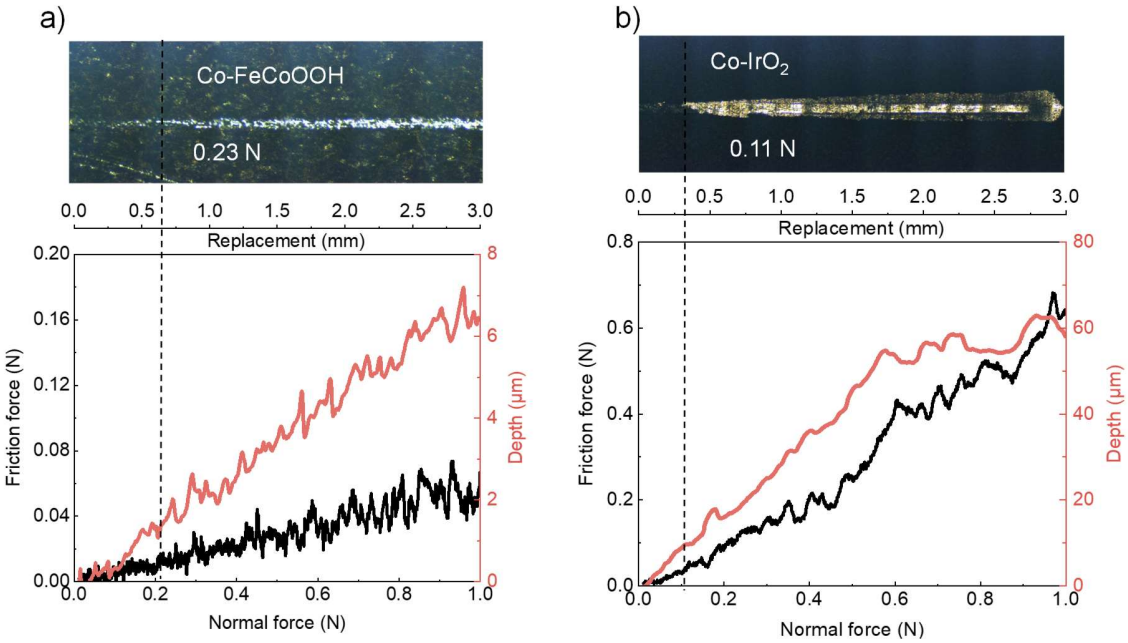

Figure S3. The photos of micro-scratches, and friction force-normal force curves of Co-FeCoOOH (a) and (b) Co-IrO_2 (b).

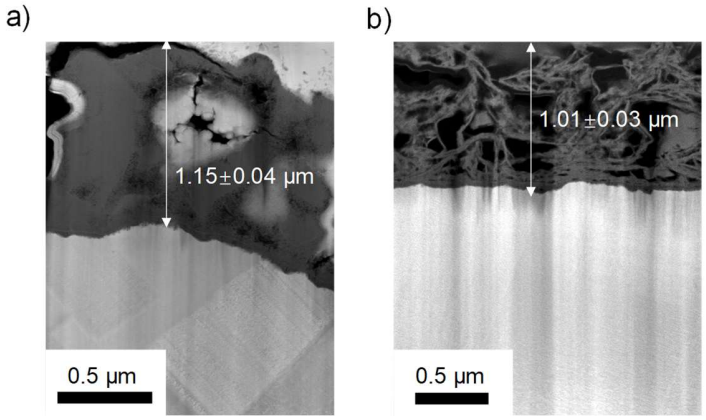

Figure S4. FIB-SEM images of cross section of a) Co-FeCoOOH and b) Co-IrO_2.

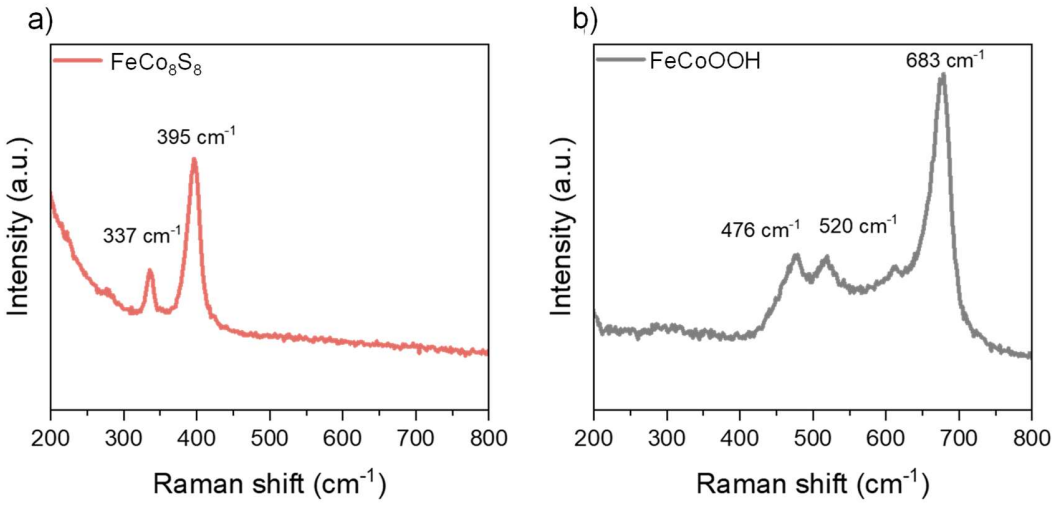

Figure S5. The Raman spectra of Co-$FeCo_8S_8$ (a) and FeCoOOH (b).

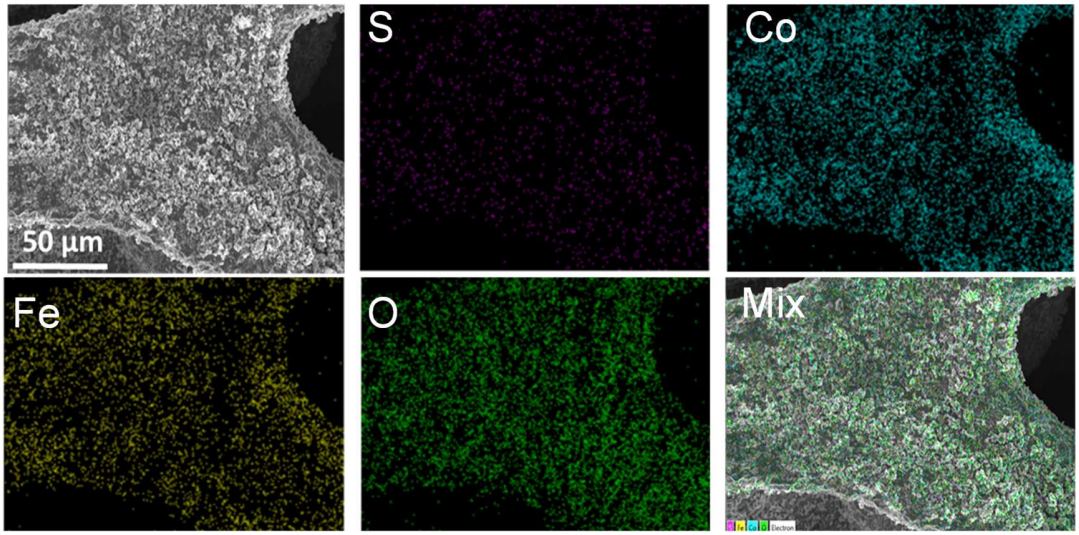

Figure S6. Energy-dispersive X-ray spectroscopy spectra of Co-FeCoOOH.

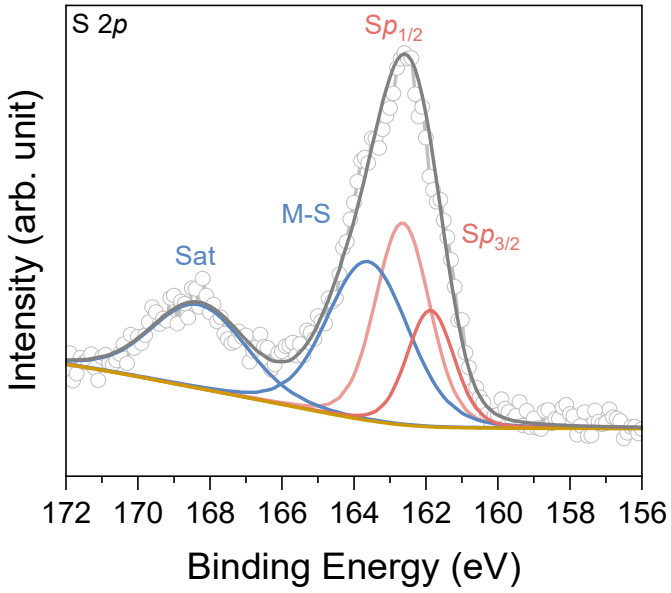

Figure S7. XPS of S 2*p* in the Co-$FeCo_8S_8$.

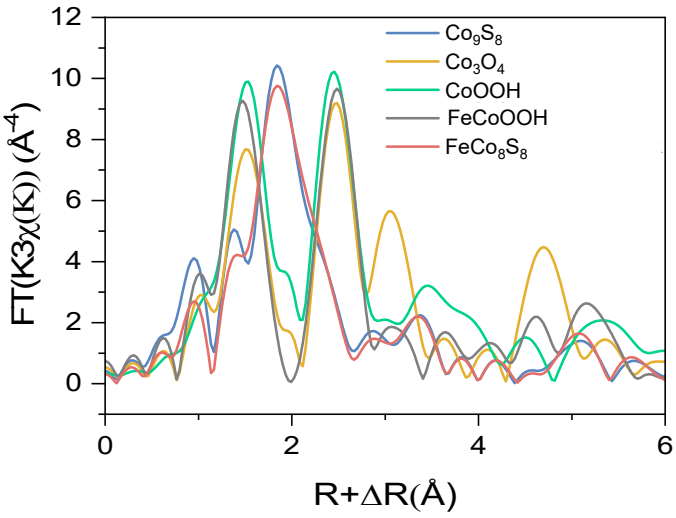

Figure S8. Fourier transform extended X-ray absorption fine structure spectra of Fe and Co *K*-edges in the $FeCo_8S_8$ and FeCoOOH.

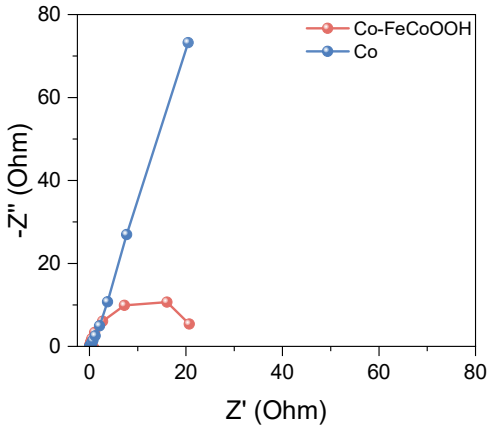

Figure S9. EIS curves of the Co-FeCoOOH and Co foam.

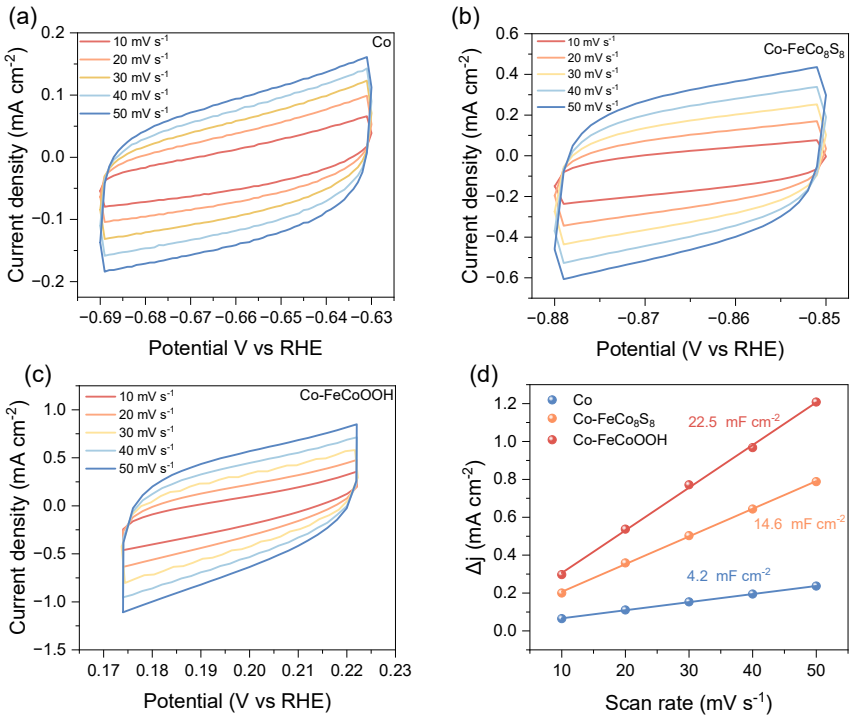

Figure S10. CV curves in the non-faradic region of (a) Co, (b) Co-$FeCo_8S_8$, and (c) Co-FeCoOOH. (d) Electrochemical double layer capacities of Co, Co-$FeCo_8S_8$ and Co-FeCoOOH (d).

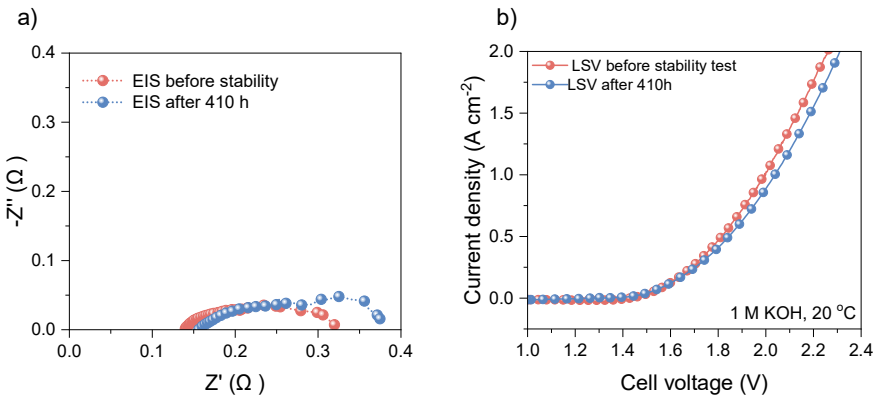

Figure S11. (a) EIS and (b) LSV curves of AEMWE before and after CP test over 400 h.

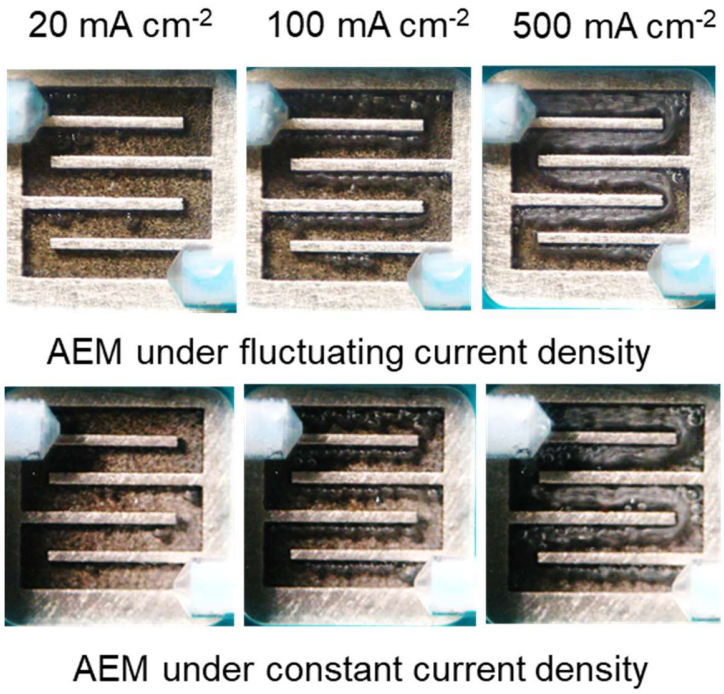

Figure S12. Images of bubble evolution of Co-FeCoOOH electrode in AEMWE under constant and fluctuating current densities.

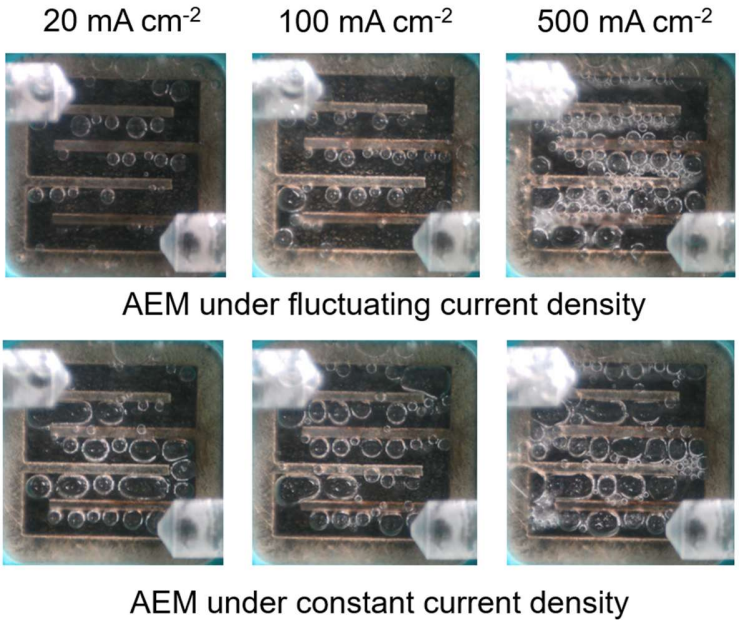

Figure S13. Images of bubble evolution of Co-IrO_2 electrode in AEMWE under constant and fluctuating current densities.

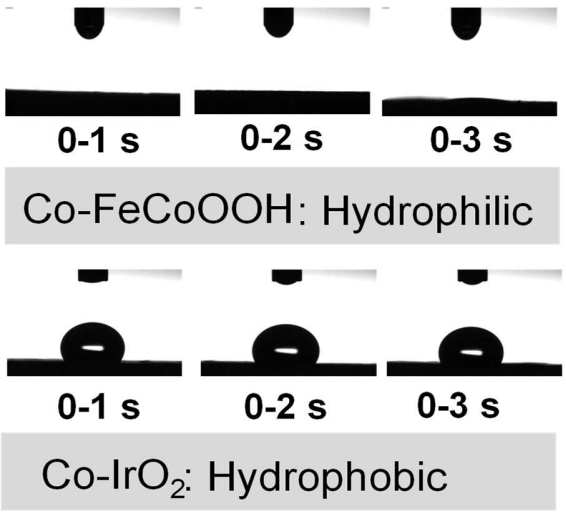

Figure S14. Comparison of contact angles of Co-FeCoOOH and Co-IrO_2.

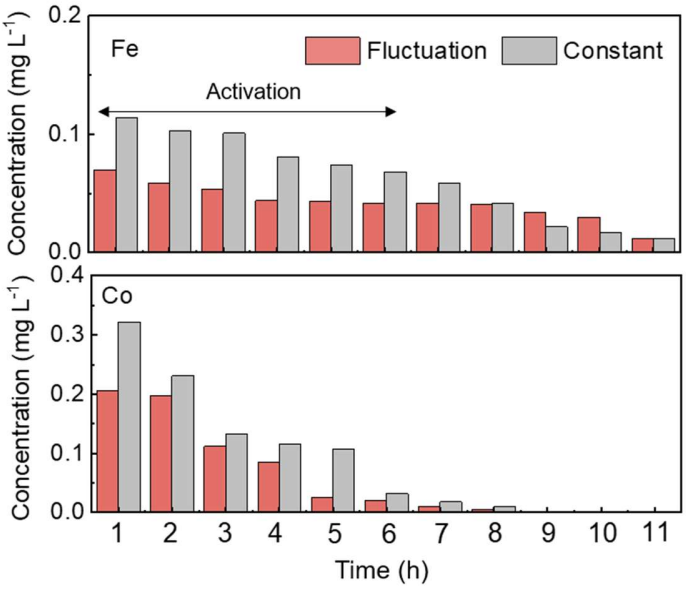

Figure S15. Comparison of inductively coupled plasma-optical emission spectrometry (ICP-OES) of Fe and Co contents in AEMWE electrolyte to study the dissolution of Fe and Co elements during constant and fluctuating current densities.

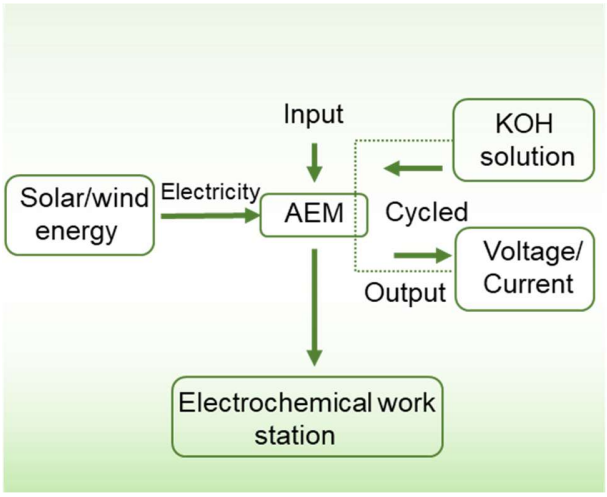

Figure S16. Schematic of Co-FeCoOOH for integrating AEMWE with solar cell.

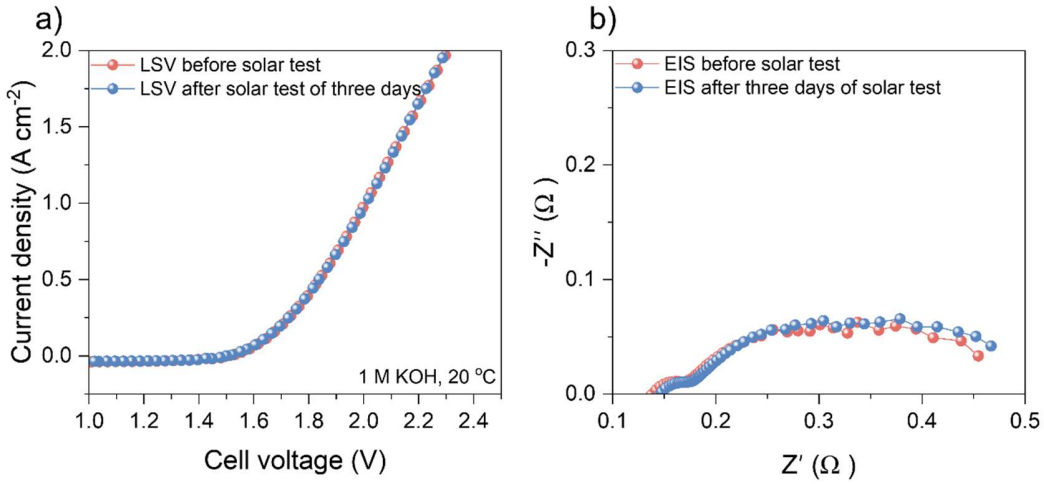

Figure S17. (a) LSV curves and (b) EIS curvses of AEMWE before and after the solar tests.

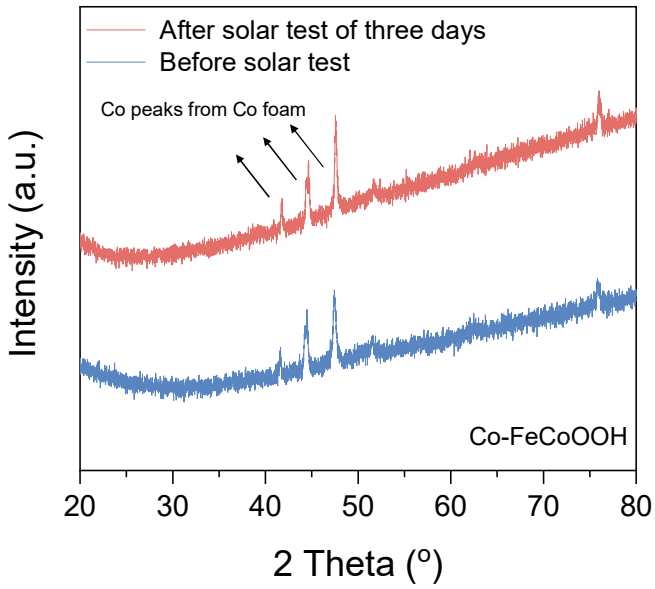

Figure S18. XRD patterns of Co-FeCoOOH before and after the solar test for three days.

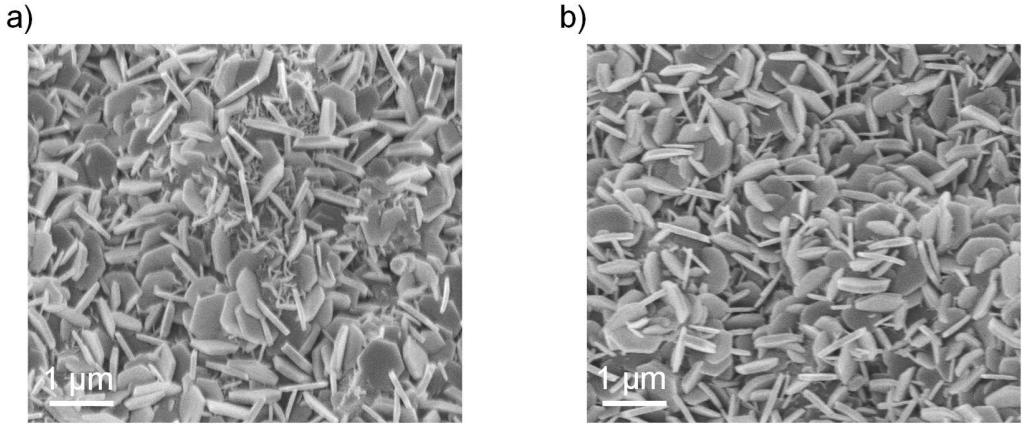

Figure S19. SEM images of Co-FeCoOOH before (a) and after (b) the solar test for three days.

Table S1. Performance comparisons of Co-FeCoOOH with other catalysts for OER at high current density ≥ 500 mA cm^{-2}

Electrodes	Electrolyte	Substrate	Performance	Durability	Refs.
$Fe_2O_3/Ni(OH)_2/NF$	1M KOH	Nickel Foam	1,500 mA cm^{-2}; 341 mV	17 h; 1,500 mA cm^{-2}	2
Ni oxyhdroxide @NiFe	1M KOH	Nickel Foam	1,000 mA cm^{-2}; 258 mV	120 h; 1,000 mA cm^{-2}	3
$Fe_{1-x}Ni_x(PO_3)_2$/ Ni_2P	1M KOH	Nickel Foam	1,000 mA cm^{-2}; 318 mV	80 h; 1,000 mA cm^{-2}	4
Ni-Fe-OH @Ni_3S_2/NF	1M KOH	Nickel Foam	500 mA cm^{-2}: 370 mV	500 h; 1,000 mA cm^{-2}	5
FCN-MOF/NF	1M KOH	Nickel Foam	1,000 mA cm^{-2}; 284 mV	50 h; 1,000 mA cm^{-2}	6
Fe-CoP/NF	1M KOH	Nickle Foam	1,000 mA cm^{-2}; 428 mV	30 h; 1,000 mA cm^{-2}	7
$NiSe_2/NiFe_2Se_4$ @NiFe	1M KOH	Nickel Iron alloy	1,000 mA cm^{-2}; 400 mV	10 h; 1,000 mA cm^{-2}	8
Ni_3N|NiFeP/FF	1M KOH	Iron Foam	500 mA cm^{-2}; 287 mV	120 h; 800 mA cm^{-2}	9
C-$Ni_{1-x}O$/3DPNi	1M KOH	3D printed nickel foam	1,000 mA cm^{-2}; 425 mV	60 h; 600 mA cm^{-2}	10
$NiMoO_x$/NiMoS array on Ni	1M KOH	Nickel Foam	1,000 mA cm^{-2}; 334 mV	500 h; 500 mA cm^{-2}	11
$NiFeO_xH_y$	1M KOH	Nickel Foam	1,000 mA cm^{-2}; 313 mV	500 h; 500 mA cm^{-2}	12
Co-NiO/Fe_2O_3	1M KOH	Nickel Foam	500 mA cm^{-2}; 230 mV	300 h; 500 mA cm^{-2}	13

$CoMoS_x$/NF	1M KOH	Nickel Foam	500 mA cm^{-2}; 351 mV	100 h; 500 mA cm^{-2}	14
NiFe/Ni/Ni	1M KOH	3D nickle mesh	500 mA cm^{-2}; 300 mV	72 h; 500 mA cm^{-2}	15
FeP/Ni_2P on Ni	1M KOH	Nickel Foam	1,277 mA cm^{-2}; 300 mV	40 h; 500 mA cm^{-2}	16
NiO/$NiFe(OH)_2$	1M KOH	Nickel Foam	500 mA cm^{-2}; 255 mV	24 h; 500 mA cm^{-2}	17
$Fe(PO_3)_2$/Ni_2P	1M KOH	Nickel Foam	500 mA cm^{-2}; 265 mV	20 h; 500 mA cm^{-2}	18
$NiFe(OH)_x$/FeS/ IF	1M KOH	Iron Foam	500 mA cm^{-2}; 304 mV	70 h; 300 mA cm^{-2}	19
Co-FeCoOOH	1M KOH	Cobalt foam	1,000 mA cm^{-2}; 311 mV	200 h; 1,000 mA cm^{-2}	**This work**
Co-FeCoOOH	1M KOH	Cobalt foam	2,000 mA cm^{-2}; 334 mV	150 h; 2,000 mA cm^{-2}	**This work**

Table S2. Stability comparisons of Co-FeCoOOH with other catalysts from the past year.

Electrodes	Current density of stability test (mA cm^{-2})	stability test time (h)	Refs
CoN/VN@NF	500	1000	20
Ni(Fe) MOF /$NiMoO_x$	500	300	21
	1000	160	
RuZn-Co_3O_4	500	100	22
Bi/$BiCeO_{1.8}H$	1000	100	23
UP-RuNiSAs/C	1000	250	24
$CoCrO_x$	500	120	25
HEMS	500	100	26
FeCoNiMnCr	100	24	27
Fe, F-CoO NNAs	500	300	28
Co-FeCoOOH	**500**	**1500**	**This work**
	1000	**200**	
	2000	**150**	

Table S3. AEMWE performance comparisons with the literature reported from the past year.

Electrodes	**Cell voltage at 1 A cm^{-2} (V)**	**Degradation rate (mV h^{-1})**	**Refs**
CoN/VN@NF	1.84	0.13	29
CAPist-L1	1.63	0.05	30
Ni(Fe) MOF /$NiMoO_x$	1.79	0.267	31
RuZn-Co_3O_4	1.84	1.30	32
LFA(NiFe)	1.83	0.11	33
Bi/$BiCeO_{1.8}H$	1.79	0.40	34
UP-RuNiSAs/C	1.95	0.228	35
$CoCrO_x$	1.98	5.40	36
HEMS	2.15	0.526	37
Co-FeCoOOH	**1.79**	**0.113**	**This work**

Table S4. Stability comparisons of Co-FeCoOOH with other catalysts at 500 mA cm^{-2}.

Materials	Stability time (h)	Refs.
V-NiFeOOH	250	38
FeO_xH_y (Fe@Co)	200	39
NiFeCoOOH	300	40
NiFeCo-Ni	400	41
$NiFe_2O_4$	500	42
FeNi LDH	180	43
P-CoVO	1000	44
Co-FeCoOOH	410	**This work**

References

1. Y. Luo, Z. Zhang, F. Yang, J. Li, Z. Liu, W. Ren, S. Zhang and B. Liu, *Energy & Environmental Science*, 2021, **14**, 4610-4619.
2. A. Kong, H. Zhang, Y. Sun, Y. Lv, M. Liu, H. Li, Y. Wang, Y. Fu, H. Zhang, W. Li and J. Zhang, *Applied Surface Science*, 2023, **613**, 156023.
3. C. Liang, P. Zou, A. Nairan, Y. Zhang, J. Liu, K. Liu, S. Hu, F. Kang, H. J. Fan and C. Yang, *Energy & Environmental Science*, 2020, **13**, 86-95.
4. Z.-J. Gong, Z.-C. Hu, Z.-J. Bai, X.-A. Yu, Z. Liu and Y.-Q. Wang, *Inorganic Chemistry*, 2023, **62**, 13338-13347.
5. X. Zou, Y. Liu, G.-D. Li, Y. Wu, D.-P. Liu, W. Li, H.-W. Li, D. Wang, Y. Zhang and X. Zou, *Advanced Materials*, 2017, **29**, 1700404.
6. D. Senthil Raja, C.-L. Huang, Y.-A. Chen, Y. Choi and S.-Y. Lu, *Applied Catalysis B: Environmental*, 2020, **279**, 119375.
7. L.-M. Cao, Y.-W. Hu, S.-F. Tang, A. Iljin, J.-W. Wang, Z.-M. Zhang and T.-B. Lu, *Advanced Science*, 2018, **5**, 1800949.
8. J. Yuan, X. Cheng, H. Wang, C. Lei, S. Pardiwala, B. Yang, Z. Li, Q. Zhang, L. Lei, S. Wang and Y. Hou, *Nano-Micro Letters*, 2020, **12**, 104.
9. J. Li, M. Song, Y. Hu, Y. Zhu, J. Zhang and D. Wang, *Small Methods*, 2023, **7**, 2201616.
10. T. Kou, S. Wang, R. Shi, T. Zhang, S. Chiovoloni, J. Q. Lu, W. Chen, M. A. Worsley, B. C. Wood, S. E. Baker, E. B. Duoss, R. Wu, C. Zhu and Y. Li, *Advanced Energy Materials*, 2020, **10**, 2002955.
11. P. Zhai, Y. Zhang, Y. Wu, J. Gao, B. Zhang, S. Cao, Y. Zhang, Z. Li, L. Sun and J. Hou, *Nature Communications*, 2020, **11**, 5462.
12. J. Liu, W. Du, S. Guo, J. Pan, J. Hu and X. Xu, *Advanced Science*, 2023, **10**, 2300717.
13. Y. Lin, X. Fan, M. Huang, Z. Yang and W. Zhang, *Chemical Science*, 2022, **13**, 7332-7340.
14. X. Shan, J. Liu, H. Mu, Y. Xiao, B. Mei, W. Liu, G. Lin, Z. Jiang, L. Wen and L. Jiang, *Angewandte Chemie International Edition*, 2020, **59**, 1659-1665.

15. P.-c. Wang, L. Wan, Y.-q. Lin and B.-g. Wang, *ChemSusChem*, 2019, **12**, 4038-4045.
16. F. Yu, H. Zhou, Y. Huang, J. Sun, F. Qin, J. Bao, W. A. Goddard, S. Chen and Z. Ren, *Nature Communications*, 2018, **9**, 2551.
17. P. Liu, B. Chen, C. Liang, W. Yao, Y. Cui, S. Hu, P. Zou, H. Zhang, H. J. Fan and C. Yang, *Advanced Materials*, 2021, **33**, 2007377.
18. H. Zhou, F. Yu, J. Sun, R. He, S. Chen, C.-W. Chu and Z. Ren, *Proceedings of the National Academy of Sciences*, 2017, **114**, 5607-5611.
19. S. Niu, W.-J. Jiang, T. Tang, L.-P. Yuan, H. Luo and J.-S. Hu, *Advanced Functional Materials*, 2019, **29**, 1902180.
20. Z. Liang, D. Shen, Y. Wei, F. Sun, Y. Xie, L. Wang and H. Fu, *Advanced Materials*, 2024, **36**, 2408634.
21. Y. Li, L. Yang, X. Hao, X. Xu, L. Xu, B. Wei, Z. Chen, *Angewandte Chemie International Edition*, 2024, e202413916.
22. G. Zhang, J. Pei, Y. Wang, G. Wang, Y. Wang, W. Liu, J. Xu, P. An, H. Huang, L. Zheng, S. Chu, J. Dong, J. Zhang, *Angewandte Chemie International Edition*, 2024, **63**, e202407509.
23. S. Jo, J. I. Jeon, K. H. Shin, L. Zhang, K. B. Lee, J. Hong, J. I. Sohn, *Advanced Materials*, 2024, **36**, 2314211.
24. Yao, R., Sun, K., Zhang, K., Wu, Y., Du, Y., Zhao, *Nature Communications*, 2024, **15**, 2218.
25 Li S, Liu T, Zhang W, Wang M, Zhang H, Qin C, Zhang L, Chen Y, Jiang S, Liu D, Liu X, *Nature Communications*, 2024, **15**, 3416.
26 Qian F, Peng L, Cao D, Jiang W, Hu C, Huang J, Zhang X, Luo J, Chen S, Wu X, Song L, *Joule*, 2024, **8**, 2342-56.
27 Hu J, Guo T, Zhong X, Li J, Mei Y, Zhang C, Feng Y, Sun M, Meng L, Wang Z, Huang B, *Advanced Materials*, 2024, **36** , 2310918.
28 Ye P, Fang K, Wang H, Wang Y, Huang H, Mo C, Ning J, Hu Y, *Nature Communications*, 2024, **15**, 1012.
29 Liang Z, Shen D, Wei Y, Sun F, Xie Y, Wang L, Fu H, *Advanced Materials*, 2024, 2408634.

30 Li Z, Lin G, Wang L, Lee H, Du J, Tang T, Ding G, Ren R, Li W, Cao X, Ding S, Ye W, Yang W, Sun L, *Nature Catalysis,* 2024*,* **7**, 944-952.

31 Li Y, Yang L, Hao X, Xu X, Xu L, Wei B, Chen Z, *Angewandte Chemie International Edition*, e202413916.

32 Zhang G, Pei J, Wang Y, Wang G, Wang Y, Liu W, Xu J, An P, Huang H, Zheng L, Chu S, *Angewandte Chemie International Edition*, 2024, e202407509.

33 Wang J, Liang C, Ma X, Liu P, Pan W, Zhu H, Guo Z, Sui Y, Liu H, Liu L, Yang C, *Advanced Materials*, 2024, **36**, 2307925.

34 Jo S, Jeon JI, Shin KH, Zhang L, Lee KB, Hong J, Sohn JI, *Advanced Materials*, 2024, 2314211.

35 Yao R, Sun K, Zhang K, Wu Y, Du Y, Zhao Q, Liu G, Chen C, Sun Y, Li J, *Nature Communications*, 2024, **15**, 2218.

36 Li S, Liu T, Zhang W, Wang M, Zhang H, Qin C, Zhang L, Chen Y, Jiang S, Liu D, Liu X, *Nature Communications*, 2024, **15**, 3416.

37 Qian F, Peng L, Cao D, Jiang W, Hu C, Huang J, Zhang X, Luo J, Chen S, Wu X, Song L, *Joule*, 2024, **8**, 2342-56.

38 P. Thangavel, H. Lee, T. H. Kong, S. Kwon, A. Tayyebi, J.-h. Lee, S. M. Choi and Y. Kwon, *Advanced Energy Materials*, 2023, **13**, 2203401

39 S. Han, H. S. Park and J. Yoon, *Chemical Engineering Journal*, 2023, **477**, 146713.

40 J. S. Ha, Y. Park, J.-Y. Jeong, S. H. Lee, S. J. Lee, I. T. Kim, S. H. Park, H. Jin, S. M. Kim, S. Choi, C. Kim, S. M. Choi, B. K. Kang, H. M. Lee and Y. S. Park, *Advanced Science*, 2024, **11**, 2401782.

41 A. Riaz, Z. Fusco, F. Kremer, B. Gupta, D. Zhang, C. Jagadish, H. H. Tan and S. Karuturi, *Advanced Energy Materials*, 2024, **14**, 2303001.

42 K. Y. Yoon, K. B. Lee, J. Jeong, M.-J. Kwak, D. Kim, H. Y. Roh, J. H. Lee, S. M. Choi, H. Lee and J. Yang, *ACS Catalysis*, 2024, **14**, 4453-4462.

43 L. Wan, Z. Xu and B. Wang, *Chemical Engineering Journal*, 2021, **426**, 131340.

44 Z. Liang, D. Shen, Y. Wei, F. Sun, Y. Xie, L. Wang and H. Fu, *Advanced Materials*, 2024, 2408634.